Chapter 23
Single–Band and Multiband Angular Filtering Using Two–Dimensional Photonic Crystals and One–Layer Gratings

Andriy E. Serebryannikov and Ekmel Ozbay

23.1   Introduction

Filtering as a process is commonly known for electrical engineers and physicists. In wide sense, it means an electrical or electronic circuit or an optical structure transmits or not electrical signals or electromagnetic waves in some ranges of variation of a selected physical parameter, but not to others. Frequency-domain filters are best known and most widely used. Their common function is to transmit or reflect in a designer-defined frequency range. The main types include bandpass, low-pass, bandstop, and high-pass filters, which function depending on which parts of the frequency spectrum should be transmitted or reflected. Sharp boundaries between pass and stop bands, total transmission in pass bands, and total reflection in stop bands are the general criteria that determine the quality of performance of any filter.

Similarly, filtering can be realized in other domains, i.e., at variations of another physical parameter while frequency is fixed. In spatial filtering, directions of incidence are assumed to be variable, whereas angular filtering represents its simplified version, in which incidence angle is varied in plane only. The spatial (angular) filters are demanded for different applications that include but are not restricted to the analysis and modification of spatial (angular) spectrum, radar data processing, aerial imaging, distinguishing the incoming waves depending on source location, detection of extrasolar planets, and biomedical applications. The known theoretical and experimental performances of spatial and angular filters include

A.E. Serebryannikov (✉)
Faculty of Physics, Adam Mickiewicz University, Umultowska 85, 61-614 Poznan, Poland
e-mail: andser@amu.edu.pl

E. Ozbay
Nanotechnology Research Center – NANOTAM, Bilkent University, 06800 Ankara, Turkey
e-mail: ozbay@bilkent.edu.tr

interference patterns [1], anisotropic media [2], grating-based resonant systems [3, 4], multilayer stacks combined with a prism [5], metallic grids backed by a ground plane [6], axisymmetric photonic microstructures [7], and various photonic crystals (PhCs) [8–12] including their microwave [13] and sonic [14] analogs that represent two-dimensional arrays of the rods. To time, both transmission-mode and reflection-mode angular filters have been proposed. The coexistence of spatial (angular) and frequency-domain filtering is an important theoretical and practical extension [4, 11]. Another aspect is related to angle-tolerant frequency-domain filtering [15, 16]. While the principal possibility of rather strong sensitivity of transmission and reflection to incidence angle variations is quite evident, the main problem is how to fulfill the general requirements regarding sharpness of the band boundaries and constant efficiency within a band, e.g., see Refs. [8, 11, 15, 16]. Indeed, any structure or medium with dispersion properties different from the host medium (usually air) is sensitive to variations in incident angle, so transmission and/or reflection is modulated. It is more difficult to entirely suppress transmission or reflection in a wide range of the angle variation. And even more difficult is to keep the constant efficiency within a band.

In this chapter, we demonstrate how all the main types of angular filtering can be achieved in transmission mode in wide bands with the aid of the structures based on two-dimensional PhCs. Transmission mode utilizes specific dispersion properties of Floquet–Bloch modes and, hence, behavior of equifrequency dispersion contours (EFCs) in the entire wavevector space. Moreover, for finite-thickness slabs of PhC, obtainable dispersion can yield unusual Fabry–Perot transmission, which is particularly appropriate for wideband angular filtering. From this perspective, PhCs represent simple and very suitable platform for angular filtering, because of suggesting a rich variety of dispersion types usable for angular filtering. Similarly to our earlier studies [8, 11, 17], the structures considered here are assumed to be made of conventional isotropic, passive dielectric materials and, thus, are easily realizable. For the sake of completeness, we also consider reflection-mode angular filtering in reflector-backed single-layer gratings, which is inspired by reflection mode of PhC gratings.

The chapter is organized as follows:

1. In Sect. 23.2, angular selectivity achievable in a classical Fabry–Perot etalon is considered.
2. Section 23.3 presents an overview of advanced Fabry–Perot regimes in slabs of PhC that are applicable to angular filtering.
3. In Sect. 23.4, the basic types of wideband angular filtering achievable in transmission mode with the aid of PhCs are considered.
4. Section 23.5 is dedicated to reflection-mode wideband angular filtering in single-layer gratings.
5. Section 23.6 briefly explains connection of angular filtering to other well-known phenomena and operation regimes.
6. Finally, concluding remarks are given in Sect. 23.7.

All the electromagnetic waves considered are assumed to be plane and monochromatic; ε_r and μ_r stand for relative permittivity and relative permeability, respectively.

23.2   Fabry–Perot Etalon and Angular Filtering

First, we consider the basic features of transmission in case of Fabry–Perot etalon that is probably the simplest example of a transmission-mode angular filter. The structure considered here represents a homogeneous dielectric slab with non-corrugated interfaces; see Fig. 23.1, inset. A well-known formula allows one to express transmittance, T, via characteristics of the slab and its interfaces [18]:

$$T = (1 - \hat{R})^2/[(1 - \hat{R})^2 + 4\hat{R}\sin^2(nkD\cos\theta')], \tag{23.1}$$

where $k = k_0 = \omega/c$ is free-space wave number, θ' is angle of refraction at the air-dielectric interface, D is the slab thickness, and n is index of refraction of the slab material. Reflectance of an air-dielectric interface, $\hat{R}$, is given by

$$\hat{R} = [(\cos\theta - n\cos\theta')/(\cos\theta + n\cos\theta')]^2, \tag{23.2}$$

where $n\cos\theta' = \sqrt{n^2 - \sin^2\theta}$ and θ is angle of incidence. Transmittance is maximal when $\sin(nkD\cos\theta') = 0$. It is assumed that the slab is made of a conventional non-dispersive, isotropic, lossless dielectric with $\varepsilon_r > 1$ and $\mu_r = 1$, i.e., $n = \sqrt{\varepsilon_r}$.

Figure 23.1 presents three examples of behavior of T in (kD, θ)-plane. Calculations are carried out by using Eq. (23.1). The basic effects caused by variations in θ, kD, and ε_r are clearly seen. They include enhancement of the effect of θ on location of the maxima and minima of T at larger values of θ and kD, disappearance of overlapping of the neighboring Fabry–Perot resonances and weakening sensitivity to variations in θ at increasing ε_r, and upshift of the resonance frequencies at increasing θ that leads to the *positive slope* of the mountains of $T = 1$ [i.e., $d\theta/d(kD) > 0$ at the mountain top] and valleys of $\min T$ between them. It is worth noting that avoiding resonance overlapping and, thus, good separation of the neighboring mountains of $T = 1$ invoke high-permittivity dielectric materials, which are available not for all parts of the electromagnetic spectrum and may show high losses.

Let us consider the features observed in Fig. 23.1 from the angular filtering perspective. The fundamental difference between the frequency-domain and angle-domain behavior of T, which may, in principle, be realized in Fabry–Perot etalon, is that there is an infinite number of the maxima of $T = 1$ in the frequency domain at fixed θ, whereas the number of the maxima in the angle domain at fixed kD can vary from zero [e.g., at $kD = 16.8$ and $\varepsilon_r = 60$ in Fig. 23.1c] to several ones [e.g., eight maxima at $kD = 58.7$ and $\varepsilon_r = 2.1$ in Fig. 23.1a], when $0 < \theta < 80°$. For low-pass
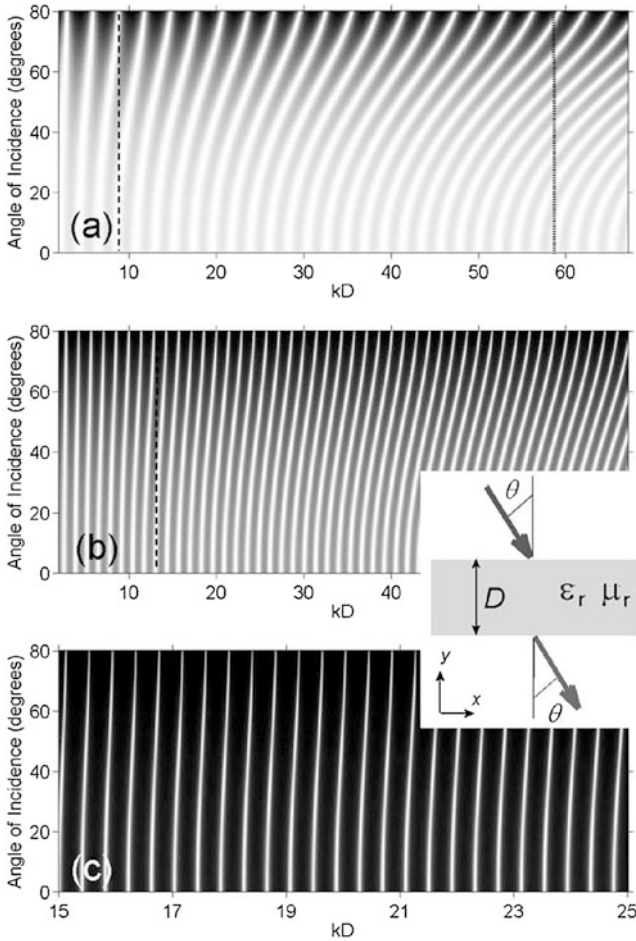
Fig. 23.1 Transmittance in (kD, θ)-plane for Fabry–Perot etalon at (**a**) $\varepsilon_r = 2.1$, (**b**) $\varepsilon_r = 5.8$, (**c**) $\varepsilon_r = 60$; *black* and *white colors* correspond to $T = 0$ and $T = 1$, respectively; different ranges of kD-variation are used in (**a, b**) and (**c**) to show details important for angular filtering; (**a, b**) only one maximum of T occurs in θ-domain at kD-values on the *left side* from *dashed line*; (**a**) *dotted line* – example of several (here – eight) maxima of T at $kD = $ const; *inset* – general geometry

angular filtering, which is the simplest regime, it is difficult to obtain a single pass band that is well separated from the bands corresponding to the neighboring maxima of T and simultaneously has a sharp boundary between high-T and low-T regimes at given $\theta = \theta_c$, while using low-permittivity dielectric materials, see Fig. 23.1a. These materials typically do not enable a single band in the angle domain, at least in the range of high sensitivity to variations in θ, where the slope may be appropriately small.

The use of high-permittivity materials allows one to obtain a single band and good separation, but the band boundaries remain blurred, because of a large slope of the mountains of $T = 1$. Indeed, low-pass filtering can be possible for high-permittivity dielectric materials owing to good separation of the neighboring mountains, provided that the slope is sufficiently small for obtaining sharp boundaries but not so small that there might be additional bands at the same kD-value. As shown in Fig. 23.1, a larger number of non-overlapping mountains can be obtained at a fixed kD while increasing ε_r. However, the realizable slope and distance between the mountains are not appropriate to fulfill the requirements of sharpness and single maximum simultaneously. When we separate the mountains with the aid of increasing ε_r, we simultaneously increase the slope. Thus, in case of Fabry–Perot etalon, the basic requirements to an angular filter can contradict with each other. For bandpass and high-pass filtering, the problem of blurred boundaries remains. Some aspects of angular selectivity in Fabry–Perot etalon have been studied in Ref. [19]. For further evidence, Fig. 23.2 presents the examples of dependencies of T on θ
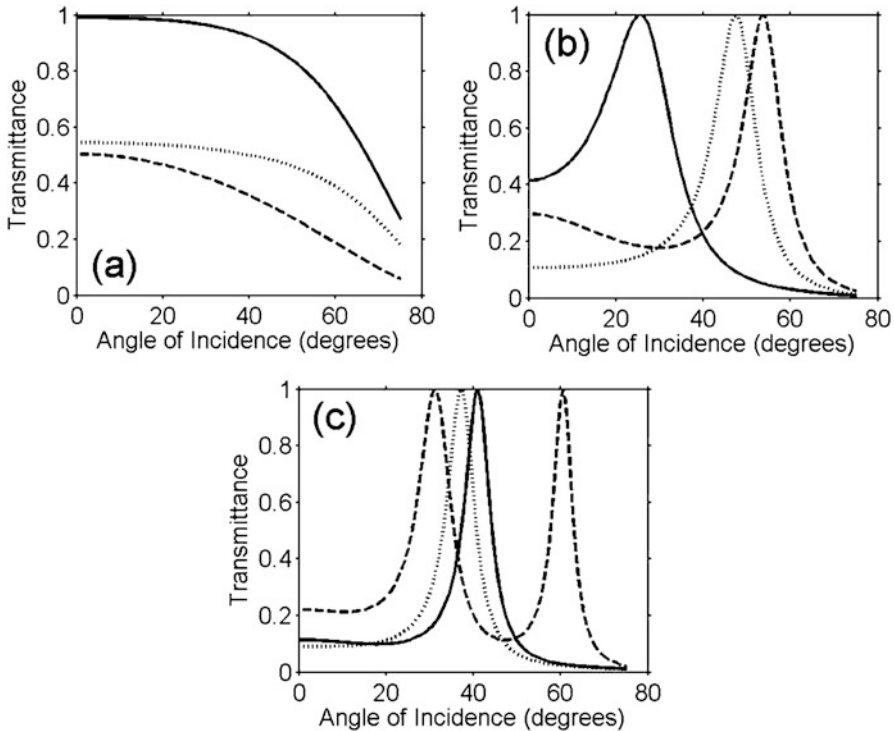

Fig. 23.2 Transmittance vs θ at fixed kD for Fabry–Perot etalon with (**a**) $kD = 2$ and $\varepsilon_r = 2.1$ (*solid line*), $\varepsilon_r = 5.8$ (*dashed line*), $\varepsilon_r = 11.9$ (*dotted line*); (**b**) $kD = 27$ and $\varepsilon_r = 16.3$ (*dashed line*), $\varepsilon_r = 35.4$ (*solid line*), $\varepsilon_r = 43$ (*dotted line*); (**c**) $kD = 51$ and $\varepsilon_r = 16.3$ (*dashed line*), $\varepsilon_r = 35.4$ (*solid line*), $\varepsilon_r = 43$ (*dotted line*)

at $kD = $ const. The problem of the blurred boundaries is clearly seen. Fabry–Perot etalon based on a low-permittivity dielectric material does not yield efficient angular filtering, see Fig. 23.2a.

If requirements to band separation and sharpness of the band boundaries are not very strict, a bell-type bandpass filter can be obtained with the aid of Fabry–Perot etalon even at $\varepsilon_r = 16.3$, as shown in Fig. 23.2b. Typically, obtaining well-pronounced angle-domain bands requires materials that have high values of ε_r. Clearly, there is no tolerance regarding choice of operation frequency in this case, because small variations in frequency can lead to unwanted deviations from the mountain top. That is why more complex approaches and structures may be required in order to obtain efficient angular filtering.

23.3   Advanced Fabry–Perot Regimes Using Photonic Crystals

As has been shown above, Fabry–Perot transmission regimes promise realization of different types of angular selectivity. In fact, the ability of homogeneous dielectric slabs to show strong selectivity in θ-domain, which is suitable for angular filtering, is connected with formation of the stop bands at large values of ε_r that occurs owing to the *impedance mismatch*. On the other hand, stop bands with sharp boundaries can be obtained with the aid of the *dispersion*-related mechanism in photonic crystals (PhCs). In this case, high-permittivity dielectric materials are not required. A rich variety of Fabry–Perot transmission regimes can be realized in finite-thickness structures based on PhCs with infinitely long rods, i.e., slabs of two-dimensional PhCs [19, 20]. It can also be achieved in PhC slabs that represent 3D structures, in which height of the rods or holes is comparable with lattice constant [21]. They may appear owing to Floquet–Bloch modes in the entirely periodic structures [19, 20], defect modes arising due to structural defects [12], and pure supercell modes, e.g., in non-uniform PhCs with parameters that are gradually varying from one unit cell to another [22]. All these structures and modes have potential in angular filtering. Moreover, in contrast with the Fabry–Perot etalon, many regimes can be realized by using PhCs made of conventional dielectric materials. Although transmission behavior of the classical Fabry–Perot etalon cannot be fully replicated in PhCs, they allow to obtain other features (e.g., sharp boundaries of the transmission bands due to the band gaps), which are highly demanded in angular filters. In fact, richness of the achievable transmission regimes is determined by richness of dispersion types in PhCs.

In the context of comparison of homogeneous dielectric slabs and finite-thickness PhCs, one should not forget that the effective boundaries of rod-type PhCs are ambiguous. This might complicate comparison of transmission in these two types of the structures. It is known that taking into account termination and matching

with the host medium is important for transmission properties of the resulting finite-thickness PhCs. In Ref. [19], multiple narrow pass bands are demonstrated for the slabs of PhCs made of conventional dielectric materials, with the aid of which, the same performance of the angular filter cannot be obtained in a homogeneous layer. It has been shown that this narrowband regime may correspond to different types of dispersion of the Floquet–Bloch modes and can be especially efficient at their band edges. Thus, narrowband angular filtering can be obtained relatively easily. This is a reason why it is worth focusing on *wideband* angular filtering.

Let us consider an example that demonstrates Fabry–Perot transmission regimes in the slabs of a square-lattice PhC (a is lattice constant) composed of the Si rods with relative permittivity $\varepsilon_r^{PhC} = 11.9$ and diameter d, see Fig. 23.3. Here and further, it is assumed that the slab is illuminated by s-polarized wave (electric field vector is parallel to the rod axes), at the angle $\theta \geq 0$, while the slab interfaces are along Γ-X direction. Two maps are presented in Figs. 23.3a and b that illustrate behavior of transmittance related to the second, third, and fourth lowest Floquet–Bloch modes (regions of $T > 0$ indicated by the numbers 2, 3, and 4, respectively). The features observed here are very general and can be obtained for various sets of PhC parameters [8, 11].

From the Fabry–Perot transmission perspective, there are three scenarios, which are distinguished in terms of sensitivity to the variations in ka and θ. Only one of them is realized in Fabry–Perot etalon. In this scenario, the mountains of $T = 1$ show the positive slope, i.e., $d\theta/d(ka) > 0$ at the mountain top. On the contrary, the scenario with the negative slope, $d\theta/d(ka) < 0$, has not been observed in Fig. 23.1. In fact, this difference indicates *positive* phase velocity in the first scenario and *negative* phase velocity (NPV) in the second one, so $\mathbf{S} \cdot \mathbf{k}^{PhC} > 0$ and $\mathbf{S} \cdot \mathbf{k}^{PhC} < 0$, respectively ($\mathbf{S}$ is the time-averaged Poynting vector, and $\mathbf{k}^{PhC}$ is the wavevector of the Floquet–Bloch mode). Finally, in the third scenario, denoted by v, there are nearly vertical mountains of $T = 1$, i.e., $|d\theta/d(ka)|$ tends to infinity. The regions of $T > 0$ in (ka, θ)-plane in Figs. 23.3a, b have sharp boundaries. Even though the neighboring mountains are not well separated from each other, the achievable Fabry–Perot transmission regimes show significant advantages compared to those in Fabry–Perot etalon. This is possible because different scenarios of transmission are realized due to Floquet–Bloch modes having different dispersion properties.

Comparing Figs. 23.3a and b, one can see that the regions of $T > 0$ in the (ka, θ)-plane have the same location, and the only significant difference is the density of the mountains of $T = 1$. This feature is exactly the same as that we would observe in two Fabry–Perot etalons that are made of the same dielectric material but have different thicknesses. Hence, the Fabry–Perot resonance nature of the mountains in Figs. 23.3a and b is evident. Thus, dependencies of T on ka obtained at $\theta = $ const while N is increased would show the same densening of the minima as that obtained for Fabry–Perot etalon while D is increased. Four examples of T vs θ are presented in Fig. 23.3c that demonstrate the principal possibility of obtaining sharp boundaries of the bands of $T > 0$ in the (ka, θ)-plane. In particular, the
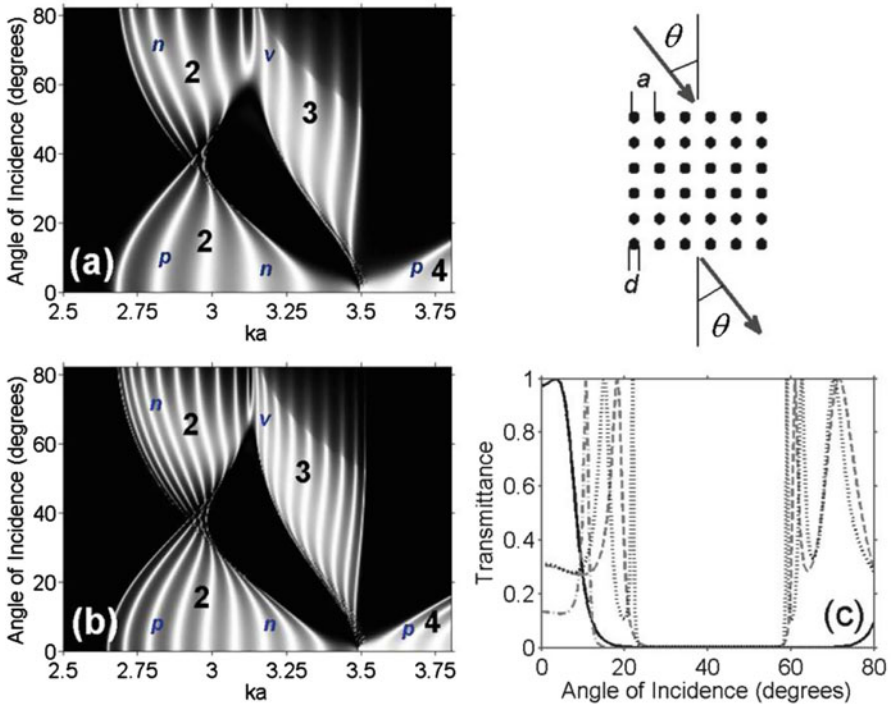
Fig. 23.3 Transmittance for slabs of PhC with $\varepsilon_r^{\text{PhC}} = 11.9$, $d/a = 0.45$ (**a, b**) in (ka, θ)-plane at (**a**) $N = 6$ and (**b**) $N = 10$; and (**c**) as a function of θ at $ka = 3.269$ (*solid line*) and $ka = 2.751$ (*dashed line*), $N = 6$, and at $ka = 2.675$ (*dash-dotted line*) and $ka = 2.751$ (*dotted line*), $N = 10$; in (**a, b**), *black* and *white colors* correspond to $T = 0$ and $T = 1$, respectively, numbers 2, 3, 4 indicate the regions in which transmission appears due to the corresponding Floquet–Bloch mode, p, n, and v indicate the regions with positive and negative slope of mountains and vertical mountains, respectively; inset shows general geometry

possibility of low-pass (solid line), imperfect narrow bandpass (dash-dotted line), and bandstop (dashed and dotted lines) filtering is demonstrated here. The case of low-pass filtering is realized for the fourth lowest Floquet–Bloch mode, while three other cases are realized for the second lowest Floquet–Bloch mode, at the lower-frequency edge of the region of $T > 0$ in (ka, θ)-plane. Clearly, fulfillment of possible requirements regarding T-values at the pass bands (e.g., $T = \text{const}$) may need other sets of parameters than in Fig. 23.3c, including ones not corresponding to the near-edge regimes. The strategy of utilizing the above discussed transmission features, which can be obtained with the aid of PhC-based structures, for different types of angular filters is considered in the next sections.

23.4 Wideband Angular Filtering in Transmission Mode

23.4.1 Basic Principles from Dispersion in k-Space

The distribution of the Floquet–Bloch modes in the *entire* wavevector space (**k**-space) determines the type(s) of angular filtering, which can be realized for a chosen set of structural parameters and frequency [11]. It is known that electromagnetic waves follow in PhC Bloch's theorem as electrons in a crystal, so the distribution of the modes in **k**-space or its two-dimensional analog, i.e., the (k_x,k_y)-plane, can be reconstructed from the distribution of the modes in the first Brillouin Zone (BZ). To do this, one should use a *repeated zone scheme* by following the symmetry of the PhC lattice similarly to the electronic case. Strictly speaking, this approach allows one to clarify whether *coupling* is, in principle, possible or impossible for a certain range of θ variation. An extensive analysis of anomalous refraction scenarios achievable in PhCs, which takes into account the mode distribution in the entire **k**-space, has first been carried out in Ref. [23]. For the purposes of angular filtering, the earlier studies of PhCs are important, because they give an idea about possible types of behavior of EFCs for PhC in **k**-space.

To obtain *wideband* angular filtering, the following requirements have to be fulfilled:

- coupling of the incident electromagnetic wave to a Floquet–Bloch wave is realized only for the desired ranges of θ-variation and forbidden otherwise;
- switching between angular pass and stop bands (the ranges of $T > 0$ and $T = 0$) must be sharp, in the ideal case – stepwise;
- constant transmission efficiency must be preserved within the entire range of $T > 0$ (in the ideal case – $T = 1$).

Let us briefly explain the meaning of these requirements in terms of properties of Floquet–Bloch modes in **k**-space. The first requirement means that EFCs of PhC must exist only within a part of the entire range of $0 < k_x < k_0$ and not exist within the remaining part, in order to enable transmission for the former and block it for the latter. The second requirement is expected to be fulfilled when EFCs tend to quickly disappear while approaching the boundary of the region of existence of a Floquet–Bloch mode in **k**-space; thickness of the slab of PhC is large enough to obtain strong energy confinement and, thus, avoid blurring of the band boundaries, and there are no surface waves or edge modes related to the finite thickness of the structure. The third requirement means, in fact, that $k_y = \text{const}$ must be obtained for EFCs in the k_x-ranges where coupling is required. It cannot be obtained in the case of circular EFCs, which correspond to the isotropic media and some of Floquet–Bloch waves in PhCs. Instead, flat EFCs are required. Generally speaking, the first requirement represents the necessary condition of dispersion-driven angular filtering in transmission mode, whereas the second and third ones determine quality of performance of an angular filter.
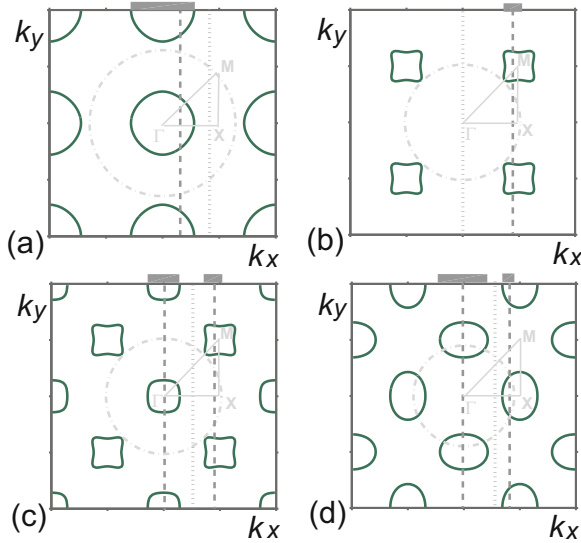
Fig. 23.4 Examples of combination of EFCs for the regular infinite PhC (*solid lines*) and air host (*dash-dotted lines – circles*) in (k_x, k_y)-plane at fixed frequency (repeated zone diagram); k_x and k_y vary from $-2\pi/a$ to $2\pi/a$; *triangles* show boundaries of the first BZ; *vertical dashed* and *dotted lines* – construction lines corresponding to the cases when coupling is and is not possible, respectively; *rectangles* at plot top schematically show location of k_x ranges, in which coupling is possible; (**a**) one nearly monotonous band solution yielding a nearly *circular* EFC around Γ-point, (**b**) one nonmonotonous band solution yielding nearly *square* EFC around M-point, (**c**) two nonmonotonous band solutions yielding nearly *square* EFCs around Γ-point and M-point, (**d**) one nonmonotonous band solution yielding *oval-shaped* EFC around X-point

Figure 23.4 presents the schematics that illustrate the coupling scenarios for some of typical shapes of EFCs for two-dimensional PhCs in (k_x,k_y)-plane at a fixed frequency. In the band regimes with monotonous (isotropic-type) dispersion, which corresponds to circular EFCs, one Floquet–Bloch wave may be coupled to the incident and outgoing waves, leading to one transmission band in θ-domain. However, if there are two band solutions, two Floquet–Bloch modes may be coupled simultaneously, resulting in two transmission bands. One band with a nonmonotonous (anisotropic) dispersion can yield either one or two transmission bands in θ-domain. More details regarding connection between behavior of EFC in **k**-space and achievable angular filtering regimes can be found in Ref. [11].

The richness of dispersion types in PhCs allows us to expect that the different types of angular filtering can be obtained even at the neighboring frequency ranges. Here, it is assumed that more than two Floquet–Bloch modes may not coexist at a fixed frequency. However, in the general case, the number of the simultaneous modes can be arbitrary.

The principal difference of the EFC-based coupling analysis carried out in **k**-space for frequency and angular filtering is that only one pair of EFCs (one EFC for

air and one for PhC) is needed in the latter case, whereas such multiple pairs are required in the former case. Thus, the coupling analysis in case of angular filtering is quite simple. Its main component, i.e., conservation of the tangential wavevector (in our case – k_x) at the slab interfaces, is common in both frequency-domain and angle-domain analysis. EFCs in air and PhC must coexist to realize coupling at given $k = k_0 = \omega/c$ and k_x and, thus, at given θ ($\sin\theta = k_x/k_0$).

In Fig. 23.4a, the coupling scenario is schematically shown, in which a Floquet–Bloch mode has isotropic-type dispersion, so the EFC is nearly circular. However, it is narrower than in air, i.e., $\max|k_x^{PhC,\Gamma}| < k_0$ (superscript Γ indicates EFC location around Γ-point), that corresponds to the index of refraction $0 < |n| < 1$. Thus, coupling is allowed by the dispersion only at $\theta < \theta_c$, $\theta_c = \arcsin(\max|k_x^{PhC,\Gamma}|/k_0)$. This results in the appearance of low-pass angular filtering at a fixed frequency. However, in Fig. 23.4a, $k_y \neq$ const at $k_x < \max|k_x^{PhC,\Gamma}|$ and, hence, $T =$ const is not expected to be realizable within the entire pass band. To obtain $T =$ const, one should have square-shaped EFCs instead of the circular ones in **k**-space. Such EFCs can be obtained in two-dimensional PhCs [31, 32].

In Fig. 23.4b, an example is presented, which corresponds to high-pass and bandpass filtering. If $\min|k_x^{PhC,M}| < k_0 < \max|k_x^{PhC,M}|$ (superscript M indicates EFC location around M-point), a coupling scenario is possible that is required for the case of high-pass filtering (shown). If $\max|k_x^{PhC,M}| < k_0 < \max k_x^{PhC,\Gamma} + 2\pi/a$, bandpass filtering is formally allowed (not shown). The PhC's EFC shape in Fig. 23.4b enables $k_y \approx$ const in a wide but not complete range of θ-variation. Thus, it is possible to obtain $T \approx$ const, according to the third requirement.

Next, the scenario in Fig. 23.4c can be appropriate for dual bandpass and bandstop angular filtering. The second (i.e., higher-θ) band is formally either bounded or not bounded at large θ, depending on whether $\max|k_x^{PhC,M}| < k_0 < \max < |k_x^{PhC,\Gamma}| + 2\pi/a$ (not shown) or $\min|k_x^{PhC,M}| < k_0 < \max|k_x^{PhC,M}|$ (shown). In the former case, it is bounded, whereas in the latter case, it is not. Clearly, $\max|k_x^{PhC,\Gamma}| < \min|k_x^{PhC,M}|$ is the necessary condition for these two types of filtering. The EFC shape in this example is suitable for obtaining $T \approx$ const. For bandstop filtering, condition $k_y =$ const is not necessary, so the requirements to the shape of PhC's EFC can be mitigated. At the same time, EFC location remains very important. An example is presented in Fig. 23.4d. The stop band may appear at θ-values corresponding to $\max|k_x^{PhC,\Gamma}| < k_x < \min|k_x^{PhC,X}|$ (superscript X indicates EFC location around X-point).

It is important that the different Floquet–Bloch modes show different types of dispersion in the same PhC [11]. This means that the different types of angular filtering may be realized in different frequency bands in *one* device that indicates new perspective routes to multiband/multifrequency operation. In fact, the abovementioned can be observed in Fig. 23.3. In this case, several types of filtering can be obtained in one structure, while only three Floquet–Bloch modes contribute to the transmission in the *ka*-range, for which $f_{\max}/f_{\min} \approx 1.4$.

23.4.2 Low-Pass Filtering

Low-pass filtering is considered to be the simplest type of angular filtering. In contrast to the other types of filtering, it can be obtained even if using a slab of a natural or artificial material with the index of refraction $0 < n < 1$. The examples include plasmas in the vicinity of plasma frequency [24], epsilon-near-zero metamaterials [25, 26], artificial ultralow-index materials [27], and natural materials showing transition from metal to dielectric state [28].

The maximal angle, at which transmission is possible, is given by

$$\theta = \theta_c = \arcsin(n). \tag{23.3}$$

In fact, low-pass filtering is based in this case on the well-known total internal reflection phenomenon, which occurs when electromagnetic wave is incident from an optically more dense medium on the interface of an optically less dense medium, e.g., see Refs. [27, 29]. However, the problem appears when $T = $ const and, in particular, when $T \approx 1$ is required within a wide range of θ-variation together with sharp switching between $T \approx 1$ and $T = 0$. Circular EFCs do not allow to obtain this regime. Clearly, the same is true for the mountains of T in case of Fabry–Perot etalon, which can be realized with the aid of the impedance mismatch mechanism at least if ε_r of the slab is rather high, see Fig. 23.1c.

While location of EFCs around Γ-point remains the necessary condition for the dispersion-based mechanism of low-pass filtering, the EFC shape is a subject of optimization. Moreover, strength of coupling is important, but it cannot be predicted based only on the dispersion results.

Figure 23.5 presents two examples of behavior of T in (ka, θ)-plane and dependence of T on θ at the selected parameter sets. Figure 23.5a corresponds to the case of nearly circular EFCs, which are expanded while ka is increased. This regime is appropriate when a narrow θ-domain passband is required. The width of the passband can be varied nearly from 2° to 7.5° ($n \approx 0.13$) by varying ka from 3.51 to 3.56. In this case, dependence of T on θ shows only one maximum. Thus, transmission through a slab of ultralow-index material can be mimicked in this case.

Figure 23.5b corresponds to the case when EFCs for the second lowest Floquet–Bloch mode are located around Γ-point but have nearly square shape. Moreover, this mode has here such properties that high transmittance is possible within a very large region in (ka, θ)-plane. After the wide ranges of $T = 1$ in θ-domain, this is the second important feature that enables efficient angular filtering with the aid of PhCs. It is not unique but needs careful parameter adjustment to be realized. In particular, large values of d/a and $\varepsilon_r^{\mathrm{PhC}}$ can be required. Note that it is important not only and mainly even not for low-pass angular filtering. In Sect. 23.4.4, its importance for dual bandpass filtering is demonstrated. In Fig. 23.5b, one has some freedom in choice of θ_c, depending on ka. However, it might be difficult to obtain a wider
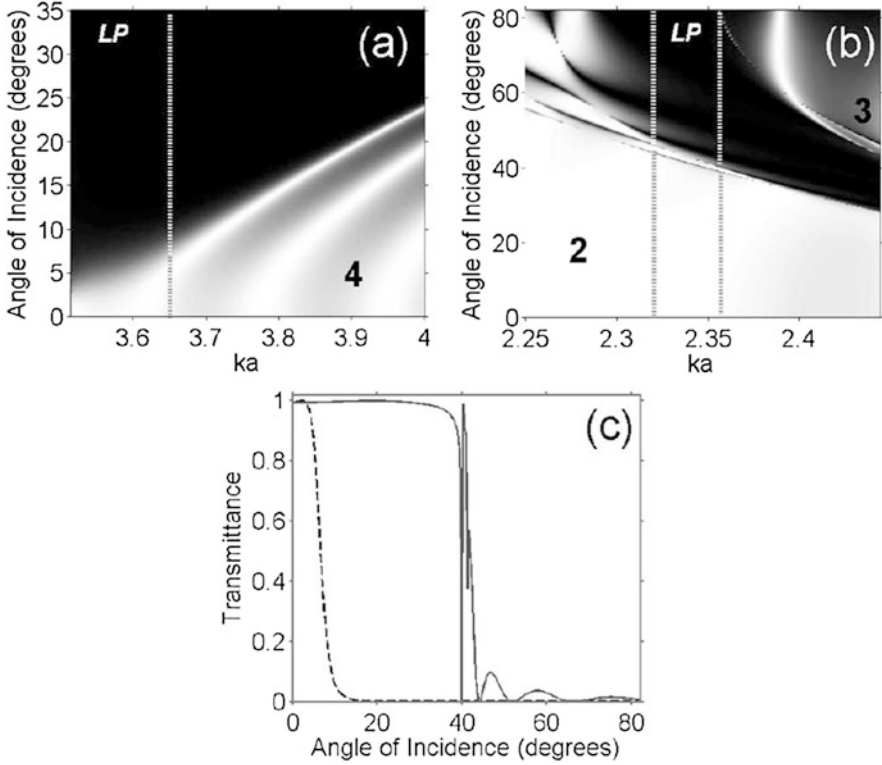
Fig. 23.5 Transmittance for slab of PhC (**a, b**) in (ka, θ)-plane at (**a**) $d/a = 0.4$ and (**b**) $d/a = 0.57$, and (**c**) as a function of θ at $ka = 2.349$, $d/a = 0.57$ (*solid line*) and $ka = 3.621$, $d/a = 0.4$ (*dashed line*); $N = 6$, $\varepsilon_r^{\mathrm{PhC}} = 11.9$; LP indicates the possibility of obtaining low-pass filtering (**a**) on the *left* to *dashed line* and (**b**) between *dashed lines*; in (**a, b**), *black* and *white colors* correspond to $T = 0$ and $T = 1$, respectively; numbers 2, 3, and 4 indicate the regions, in which transmission appears due to the corresponding Floquet–Bloch modes

ka-range suitable for low-pass filtering, since square-shaped EFCs located around Γ-point often coexist with EFCs for other Floquet–Bloch modes (or with EFCs arising due to the same mode), which contribute to transmission in unwanted ranges of θ-variation. In this case, low-pass filtering cannot be realized.

In Fig. 23.5c, T vs θ is shown in two selected cases from Figs. 23.5a and b. For the first of them (shown by solid line), we obtain $\theta_c \approx 39°$ and $|n| = 0.63$ at $ka = 2.34$. For the second one (shown by dashed line), $\theta_c < 10°$, so it is mimicking a material with $0 < n < 0.17$. Some unwanted features may appear in the θ-dependencies of T due to the edge modes (near $\theta = 40°$). In spite of this, $T \approx 1$ in a wide θ-range, as desired.

23.4.3   Bandpass and High-Pass Filtering

Indefinite media [2] and hyperbolic metamaterials [30] formally fulfill the minimal
requirements to a high-pass filter regarding EFC location. However, they typically
do not allow one obtaining $T = $ const in a wide θ-range, because $k_y = $ const
cannot be achieved in a wide range of k_x variation. It is even more difficult to obtain
bandpass filtering with a sharp upper boundary of the band at large values of θ.
Similarly to the case of low-pass filtering, we need square-shaped EFCs that should
now be located only around M-point in **k**-space. For $\varepsilon_r^{\mathrm{PhC}} = 11.9$, they can be
obtained at smaller values of d/a than in Figs. 23.3 and 23.5.

   Figure 23.6 presents the examples of behavior of T in (ka, θ)-plane and
dependence of T on θ in the selected cases. In Fig. 23.6a, one can see that bandpass
filtering can be obtained in a large region of the (ka, θ)-plane, where Fabry–
Perot transmission with the alternating mountains and valleys of T is observed.
Several mountains can be used simultaneously, i.e., efficient bandpass filtering can
be obtained at several frequencies which are quite close to each other. Since the
mountains are not sharp so there is some flexibility for fine adjustment of the ka-
value, some problems may appear at the band edges, e.g., due to dependence of
the mountain locations on ka at the lower boundary of the transmission region. It
is noteworthy that this boundary is fully determined by the properties of the third
lowest Floquet–Bloch mode. On the contrary, the upper (here – blurred) boundary
appears due to the effect of diffraction order $m = -1$. Thus, it can be approximated
at given θ by the equation

$$k_u a = 2\pi/(1 + \sin\theta), \tag{23.4}$$

which is obtained from the condition of propagation of this order [33]. In turn, for
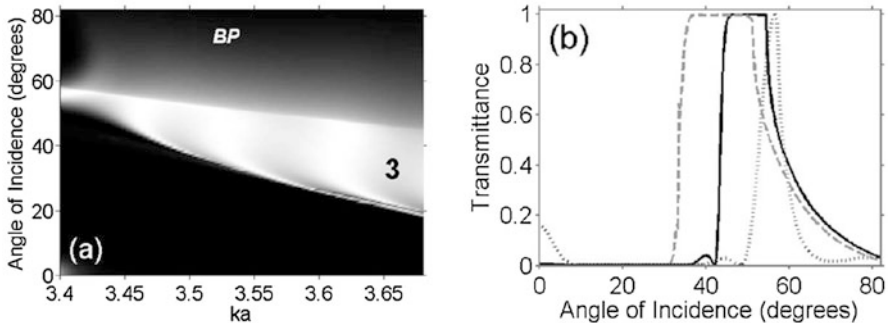given ka, $\sin\theta_u = 2\pi/(ka) - 1$.

Fig. 23.6 Zero-order transmittance for slab of PhC (**a**) in (ka, θ)-plane and (**b**) as a function of
θ at $ka = 3.463$ (*solid line*), $ka = 3.53$ (*dashed line*), and $ka = 3.412$ (*dotted line*); $N = 6$,
$d/a = 0.36$, $\varepsilon_r^{\mathrm{PhC}} = 11.9$; in (**a**), BP indicates the possibility of obtaining bandpass filtering in the
entire ka-range considered; *black* and *white colors* correspond to $T = 0$ and $T = 1$, respectively;
number 3 indicates that transmission appears due to the third lowest Floquet–Bloch mode

In fact, bandpass filtering is realized here owing to the common effect of dispersion and diffraction. Zero-order transmission above the upper boundary in Fig. 23.6a becomes weaker due to the order $m = -1$. It is worth noting that the transmission regimes realized due to the order $m = -1$ usually do not show high efficiency, so that they are of limited interest for angular filtering and, thus, are not considered here. In Fig. 23.6b, one can see the pass bands obtained at $ka = $ const. In spite of the expected difficulties at the edges, these pass bands do not strongly suffer from them. Moreover, choosing a suitable value of ka, one may vary width and location of the band. The condition of $T \approx 1$ is fulfilled in a wide θ-range, as required. For instance, $\Delta\theta \approx 15°$ for the range of $T \approx 1$ at $ka = 3.53$ and $\Delta\theta \approx 20°$ for that at $ka = 3.624$.

In the considered range of parameter variation, we have $\min|k^{\mathrm{PhC,M}}| < k_0 < \max|k^{\mathrm{PhC,M}}|$, so the contribution of the propagating order $m = -1$ is *necessary* to obtain bandpass filtering. Would this condition be satisfied while no one higher order is propagating, one should obtain rather high-pass filtering, for which coupling efficiency and transmission can be reduced at the grazing angles. The approach to obtaining the upper boundary that is realized here has been suggested in Ref. [8]. Usually, the second Floquet–Bloch mode in such a scenario, if involved, is parasitic and might not affect the principal possibility of the single bandpass filtering regime only if it is uncoupled (e.g., because of specific modal properties) to the incident wave and/or its k_x-range is entirely embedded into that of the operation mode. It is worth noting that the dispersion features required for bandpass and high-pass filtering are very general for PhCs. Many examples can be found in the literature [11, 31, 32].

23.4.4 Bandstop and Dual Bandpass Filtering

Next, we consider two types of angular filtering, which are closely related to each other: bandstop and dual bandpass filtering. Indeed, if we have two separated pass bands, there should be a stop band between them. The difference, however, is that for operation in bandpass regime, the condition of $T = 1$ is required, whereas for bandstop operation the requirements to transmittance in the neighboring pass bands can be mitigated. Following the line of reasoning from Sect. 23.4.1, it is not difficult to predict which EFCs are required: the square-shaped EFC located at Γ-point that is responsible for the low-θ pass band and the square-shaped EFC located at M-point that is responsible for the high-θ pass band. Then, the gap between the EFCs must exist that enables a stop band.

Dual bandpass filtering can be obtained when $\min|k^{\mathrm{PhC,M}}| < k_0 < \max|k^{\mathrm{PhC,M}}|$ and $\max|k^{\mathrm{PhC,\Gamma}}| < \min|k^{\mathrm{PhC,M}}|$. The first of these conditions can be modified by taking into account that the boundary of the second band in the θ-domain can be created due to the effect of a higher diffraction order.
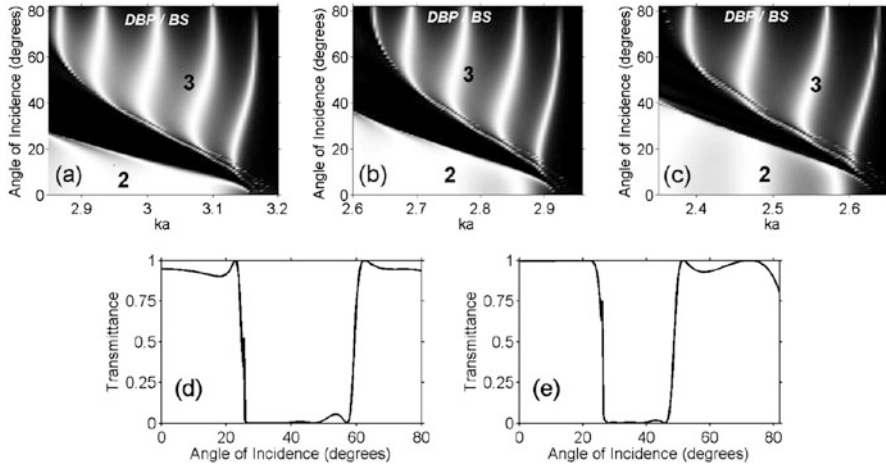
Fig. 23.7 Transmittance for slab of PhC in (ka, θ)-plane at (**a**) $d/a = 0.45$, (**b**) 0.5, and (**c**) 0.57 and as a function of θ at (**d**) $d/a = 0.45$, $ka = 2.869$ and (**e**) $d/a = 0.5$, $ka = 2.689$; $N = 6$, $\varepsilon_r^{PhC} = 11.9$. In (**a–c**), DBP and BS indicate the possibility of obtaining dual bandpass and bandstop filtering at selected values of ka and in most part of the considered ka-range, respectively, *black* and *white colors* correspond to $T = 0$ and $T = 1$, respectively; numbers 2 and 3 indicate the regions, in which transmission appears due to the corresponding Floquet–Bloch mode

Figure 23.7 presents a few examples. T in the (ka, θ)-plane is shown in Figs. 23.7a–c. The difference between the three considered structures is only in the value of d/a. One can see that the basic features are very general, i.e., they occur in a wide range of d/a-variation that provides big freedom for filter design. Transmission is obtained here due to the simultaneous contribution of the second lowest (at smaller θ) and the third lowest Floquet–Bloch mode (at larger θ). Accordingly, a stop band region size depends on how well the regions of existence of these modes in (ka, θ)-plane are separated from each other. Both types of the above discussed unusual Fabry–Perot transmission, i.e., nearly vertical mountains and wide ranges of $T \approx 1$ are presented here. For the second lowest mode, T is weakly sensitive to variations of ka and θ in a large region of the (ka, θ)-plane. Moreover, $T \approx 1$ can be preserved at least for a larger part of this region, while the case of $d/a = 0.5$ is preferable. The mountains of $T \approx 1$ can be obtained for the third lowest mode that are either totally vertical or show a very large slope. The coexistence of these two types of the unusual behavior is very important for dual bandpass filtering. Indeed, if both modes would create the alternating mountains and valleys of T in (ka, θ)-plane, an additional problem should be solved, i.e., how to match location of the mountains for two Floquet–Bloch modes. In the general case, this would be a quite challenging task. It could be even more complicated if angular filtering is required at two or more different and not close values of ka, so that the matching should simultaneously be achieved at all of these values. This cannot be done without careful parameter adjustment. Nevertheless, the principal possibility of such a matching, at least for one ka-value, has been demonstrated for the parameter set, which is similar to those used in Fig. 23.7 [8].

An alternative and more universal way of matching would need the transmission properties of the third lowest Floquet–Bloch mode that are similar to the second one. However, to time, such parameter sets are not known, and the principal possibility of realization of this case remains a subject of discussions. It is noteworthy that for the third lowest mode, most of the mountains of T show a large positive slope rather than are exactly vertical. The most appropriate of them are located closer to the left edge of the region of $T > 0$ that corresponds to this mode. Together with the possibility of matching regimes of $T \approx 1$ that are connected with different Floquet–Bloch modes, sharp (non-blurred) boundaries of the transmission bands, which are realizable due to localization of the Floquet–Bloch modes in **k**-space, represent the fundamental property enabling high performance of dual bandpass angular filters. Thus, although deviation of the mountains from the vertical position can lead to imperfectness of the transmission response in the θ-domain, it does not significantly affect the advantages of the used approach, which are connected with the specific properties of the Floquet–Bloch modes. Clearly, several regimes of dual bandpass filtering can coexist in one structure due to the same mode, but correspond to different values of ka.

Comparing Figs. 23.7a–c and 23.6a, one can see the difference in behavior of T at large values of θ. Indeed, larger values of d/a than in Fig. 23.6 are required to obtain $T \approx 1$ in wide ranges of variation in ka and θ. However, this leads to the downshift of the ka-range, in which the second and third lowest Floquet–Bloch modes coexist, while larger values of ka are required for propagation of the order $m = -1$. Hence, an additional parameter adjustment is required in order to simultaneously obtain two Floquet–Bloch modes and the propagating order $m = -1$. It is noticeable that variations in d/a may lead to strong modification of some of Floquet–Bloch modes, whereas the other ones are not so strongly affected.

Two examples of behavior of T as a function of θ are presented in Figs. 23.7d and e. In spite of some imperfectnesses that manifest themselves in a slight deviation from the regime of $T = 1$ and possible effects of edge modes, the pass and stop bands are quite well pronounced. Different combinations of the widths of the θ-domain pass bands arising due to different Floquet–Bloch modes can be realized. However, the left edge of the region of $T > 0$ in (ka, θ)-plane, which is connected with the third lowest mode, remains preferable for operation because an almost vertical mountain of $T = 1$ can be obtained in this case.

23.5 Wideband Angular Filtering in Reflection Mode

In fact, any transmission-mode angular filter can be considered at $\theta \neq 0$ as a three-port system, in which the input and output are associated with the incident and transmitted wave, respectively, while one of the ports (reflection) is blocked in the ideal case. In the general case, the output should not necessarily be connected with a transmitted wave. For reflection-mode operation, the output must be associated with one of the higher diffraction orders in reflection, into which the

incident-wave energy is entirely converted. Thus, similarity to the above considered transmission-mode filtering is only partial. Indeed, the angle at which transmitted wave propagates in the exit half-space is always given by $\phi_{\text{out}} = \theta$, while higher diffraction orders remain evanescent. In reflection mode, there is no other chance to achieve angular filtering than by means of extreme redistribution of the incident-wave energy in favor of a propagating higher order ($|m| > 0$). In the ideal case, zero-order reflectance $r_0 = 1$ at $0 < \theta < \theta_c$, where θ_c is the angle at which switching between the two orders takes place. In turn, higher-order reflectance $r_m = 1$ at $\theta_c < \theta < \theta_u$, $\theta_u < \pi/2$, $|m| > 0$. In this case, the grating theory gives [33]

$$\phi_{\text{out}} = \arcsin[\sin\theta + 2\pi m/(kL)], \qquad (23.5)$$

where L is grating period. In Ref. [34], it has been shown that efficient bandpass filtering with a sharp switching between the orders $m = 0$ and $m = -1$ can be obtained in reflection mode in rod-type PhC gratings created by introducing corrugations on a non-corrugated slab of PhC, like that in Fig. 23.3, inset, and relevant single-layer rod gratings backed with a metallic reflector. For reflector performance, it does not matter how (nearly) perfect reflections are achieved.

The main advantage of the single-layer gratings is that they suggest compact performances, which can be several times thinner than the PhC-based transmission-mode filters. In this case, the ability of keeping $r_{-1} \approx 1$ in a wide range of θ-variation may be connected rather with the specific phase and impedance conditions. However, a disadvantage of reflection mode is that the vicinity of $\theta = |\phi_{\text{out}}|$ should be excluded from the operation θ-range to avoid unwanted backward reflections. Let us assume that the incident-wave energy is perfectly converted into the order $m = -1$, i.e., $r_{-1} = 1$. Then, according to Eq. (23.5),

$$\sin\phi_{\text{out}} = \sin\theta - 2\pi/(kL). \qquad (23.6)$$

Hence, the angle between two beams is $\delta = 2\theta$ at $0 < \theta < \theta_c$ and $\delta = |\theta + \phi_{\text{out}}|$ at $\theta_c < \theta < \pi/2$ (note that $\phi_{\text{out}} < 0$ in this case). One can see that δ is a linear function of θ in the first case and a nonlinear function of θ in the second case. To compare, we have always considered $\delta = 2\theta$ for transmission mode in Sects. 23.2, 23.3, and 23.4.

Similarly to Ref. [34], nearly perfect switching between the orders $m = 0$ and $m = -1$ can be obtained in single-layer gratings in Fig. 23.8. Geometry of the problem is shown in Figs. 23.8a and b. In contrast with Ref. [34], the rods are assumed now to be square-shaped and located on a low-permittivity substrate. Figure 23.8c shows how ϕ_{out} is changed depending on whether the order $m = 0$ is only one propagating order or the order $m = -1$ also may propagate and, moreover, all energy is transferred into this order.

Figure 23.9 presents an example of reflection-mode angular filtering, which is realized with the aid of the structure that comprises the components having relative
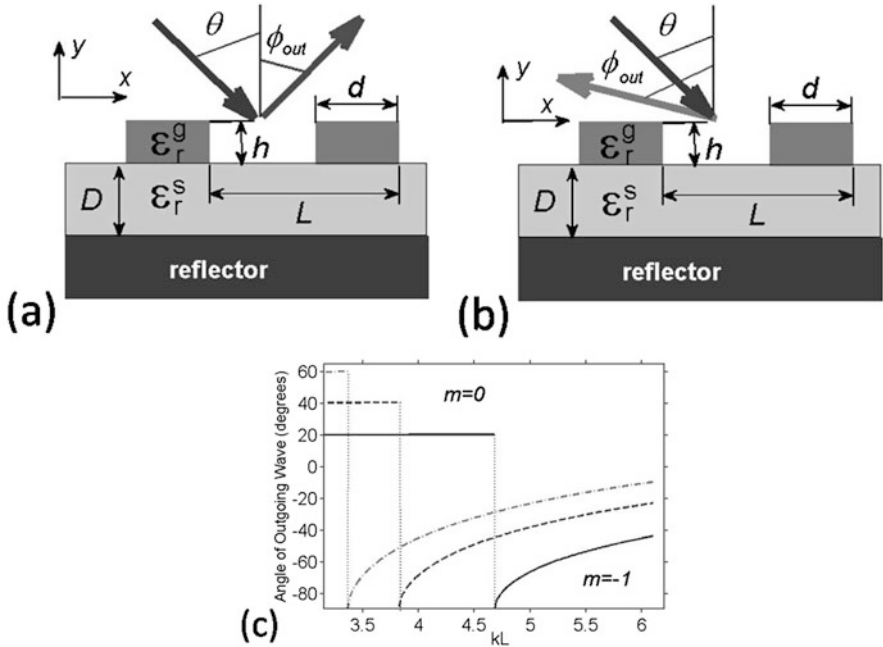
Fig. 23.8 Schematics of reflector-backed single-layer grating with (**a**) zero-order and (**b**) first-order outgoing beam; two periods over x are shown; (**c**) ϕ_{out} vs kL at $\theta = 20°$ (*solid line*), $\theta = 40°$ (*dashed line*), and $\theta = 60°$ (*dash-dotted line*) in case of ideal switching between orders $m = 0$ and $m = -1$

permittivity $\varepsilon_r^g = 5.8$ and $\varepsilon_r^s = 2.1$, and is backed by a metallic reflector. The rods of square cross section have been used in order to obtain a more feasible performance. In Fig. 23.9b, one can see that there is a very large region of $r_{-1} \approx 1$ in (kL,θ)-plane. Hence, a bandpass filter can be realized. In turn, in Fig. 23.9a, low-pass angular filtering with $r_0 \approx 1$ is observed. The pass bandwidth is determined in both cases by the condition of propagation of the order $m = -1$. In case of zero-order operation, one may introduce the equivalent index of refraction as $n_{eq} = 2\pi/(kL) - 1$, for given kL and, thus, for given θ_c. It is important that similar behavior of r_0 and r_{-1} in (kL,θ)-plane can be obtained for a very large class of the structures that include various PhC gratings and single-layer gratings.

Figure 23.9c presents dependencies of r_{-1} on θ at the selected values of kL. One can see that the lower-θ boundary is sharp, while $r_{-1} \approx 1$ is kept in a wide θ-range that extends over 40°. The total thickness of the substrate and grating is $(h + D)/\lambda \approx 0.2$ (λ is free-space wavelength) at $kL = 4.626$. In addition to the subwavelength thickness, freedom in choice of kL and, thus, operation frequency is a big advantage compared to the structures that may show a desired angular behavior only in a narrow kL-range and/or a bell-shaped pass band in θ-domain.
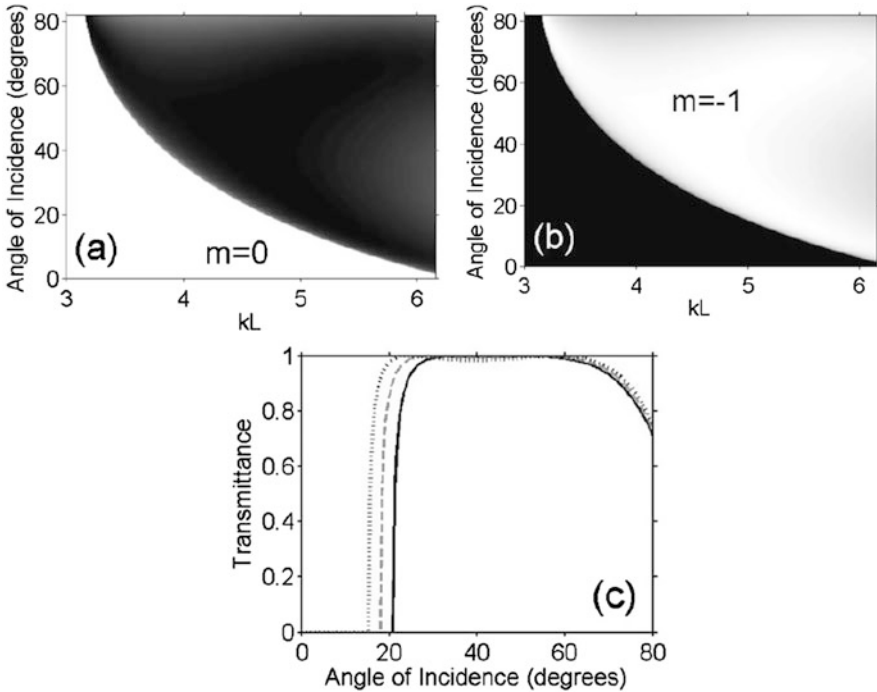
Fig. 23.9 (**a**) Zero-order and first-order reflectance (**b**) in the (kL, θ)-plane and (**c**) as a function of θ at $kL = 4.626$ (*solid line*), $kL = 4.796$ (*dashed line*) and $kL = 4.965$ (*dotted line*), for the structure shown in Fig. 23.8a, b at $h/L = 1.57 \times 10^{-1}$, $d/L = 1.96 \times 10^{-1}$ and $D/L = 1.08 \times 10^{-1}$; $\varepsilon_r^s = 2.1$, $\varepsilon_r^g = 5.8$; in (**a**), *black* and *white colors* correspond to $r_0 = 0$ and $r_0 = 1$, respectively; in (**b**), *black* and *white colors* correspond to $r_{-1} = 0$ and $r_{-1} = 1$, respectively

23.6 Connection to Other Phenomena and Operation Regimes

One of the reasons of strong interest to PhCs at the beginning of 2000s has been connected with their ability to obtain NPV, as well as *negative refraction* with or without NPV [32, 35]. For the purposes of angular filtering, shape and location of EFCs in **k**-space rather than sign of phase velocity and sign of refraction are important. Nevertheless, since the latter have often been obtained for Floquet–Bloch modes with square-shaped EFCs, efficient angular filtering can be realized in the same structures as and simultaneously with these phenomena.

On the other hand, angular filtering realized with the aid of square-shaped EFCs is connected with *collimation* inside the PhC [36]. However, angular filtering is associated rather with the selected-angle collimation, since desired angular selectivity could not be obtained in the all-angle collimation regime. In fact, this corresponds to the requirement regarding PhC's EFC that must coexist with EFC for air only in k_x ranges, where coupling is required for a particular type of angular filtering.

In this chapter, plane-wave approximation has been utilized. In case of narrow Gaussian beams, angular spectrum is wide so that some spectral components are suppressed while passing through a filter. Generally, wide spectrum leads to the blurring of the boundaries of pass and stop bands in θ-domain, e.g., see Ref. [17]. For wide pass bands and relatively narrow angular spectra, effects of blurring can be mitigated. Adjusting the widths of the pass and stop bands, one can obtain strong modulation and even splitting of the incident beam, if it has a wide angular spectrum.

Radiation from a source embedded into a slab of PhC is one more aspect of angular filtering. Indeed, what may happen when a source, i.e., a dipole or a line source is placed inside the slab? If coupling to the outgoing waves is possible only within a limited range of k_x values, in line with the necessary condition of angular filtering, radiation from such a slab is allowed only in the directions corresponding to the θ-domain pass bands. In particular, off-axis radiation can be obtained, while the total number of the radiated (on- and off-axis) beams (waves) is determined by location of EFCs in **k**-space; compare to Ref. [13].

From this perspective, *multifunctionality* realizable in transmission mode should be understood not only in sense of coexistence of different types of angular filtering in different frequency ranges but also as possible coexistence of angular filtering with other operation regimes in one structure. Due to large regions of nearly perfect transmission in (ka, θ)-plane, the studied structures and mechanism of angular filtering therein are particularly appropriate for *spatial-frequency* filtering.

The above mentioned partially remains true regarding reflection mode. In this case, total conversion of the incident-wave energy into the reflected order $m = -1$ is needed, whatever the used structure is. Clearly, redistribution of the incident-wave energy in favor of one of the higher orders is nothing else than *blazing*, a diffraction grating regime that has been well known for a long time [37–39]. The difference from the conventional blazed gratings is that we require $r_{-1} = 1$ in a wide range of θ-variation. In turn, the known performances of the blazed gratings are expected to be usable at least as narrowband angular filters. However, the θ-domain behavior has usually been not considered in the studies of the blazed gratings. Therefore, estimation of the ability of the earlier proposed diffraction gratings to function as efficient angular filters can be complicated without additional studies. It is worth noting that also for reflection mode, nearly perfect efficiency can be kept in a large region in (kL, θ)-plane, so that strong selectivity with respect to θ is expected to occur also for relatively narrow incident beams, although the boundaries of the bands can be stronger blurred in this case. When a nonsymmetric PhC grating is used in reflection mode, different regimes of diffraction inspired asymmetric transmission may appear in the neighboring frequency ranges [31, 40].

23.7   Concluding Remarks

To summarize, the main types of filtering, i.e., low-pass, bandpass, high-pass, and bandstop ones, can be realized in transmission mode in the incidence angle domain with the aid of the relatively simple structures which represent slabs of rod-type

PhCs. Either rod-type PhCs or single-layer rod gratings backed with a reflector can be used for reflection-mode operation. The utilized transmission mechanism combines the effects of dispersion of Floquet–Bloch modes and unusual Fabry–Perot resonances that cannot be obtained in Fabry–Perot etalon. At the same time, matching and mismatching to the host medium, which is the basis of angular filtering by using Fabry–Perot etalon, remains an important part of the resulting filtering mechanism in case of rod-type PhCs. In contrast with Fabry–Perot etalon, PhCs for angular filtering can be made of conventional dielectric materials and, nevertheless, enable better performance of some types of angular filters. Moreover, not all of the main types can be obtained without structuring like that in PhCs, at least if passive isotropic materials are utilized. On the other hand, structuring allows one avoiding the use of anisotropic materials.

What is probably most important is that the slabs of PhC can preserve the same (nearly unity) transmittance in a wide range of variation of the incidence angle, while frequency is fixed. This feature cannot be obtained by using homogeneous slabs of isotropic or anisotropic materials. In fact, (nearly) square shapes of EFCs in the wavevector space are needed to obtain the constant transmittance, whereas localization of Floquet–Bloch modes in this space together with some other properties may enable sharp boundaries of the pass and stop bands in transmission. Multiband (multifrequency) angular filtering, in which all the bands belong to the same type of filtering, can be obtained when several mountains of $T = 1$ of the same mode are used simultaneously. It is evident that the considered approach is very promising also for spatial-frequency filtering, so its potential should be studied deeper.

All the basic transmission and dispersion features responsible for the observed effects are very general and obtainable in PhCs for a very wide range of parameter variation. Moreover, since no diffractions are needed in transmission mode, one may expect that one-dimensional PhCs can be used at least in cases when requirements to the particular design are not very strict. Thus, various multilayer structures, which were earlier designed to operate as frequency filters, may show strong angular selectivity. However, the problem of constant transmission is not expected to be fully solvable in these structures. In reflection mode, one-dimensional periodic structures are sufficient for obtaining bandpass filtering within a wide range of the incidence angle. A deeper understanding of the physics underlying sharp switching and wide-range preserving of (nearly) unitary reflectance with the aid of a dispersion-free mechanism is desirable, since it can indicate a route to new transmission mode angular filters realizable in thinner structures than the slabs of PhCs, which have been considered here. Estimation of the potential of metasurfaces in transmission-mode angular filtering is a subject of future studies. In particular, metasurfaces controlled with the aid of magnetostatic field are very promising areas of research [41]. To date, it is not clear whether all the main types of angular filtering can be obtained in compact structures that are based on metasurfaces, whereas the potential of PhCs is well investigated. For reflection mode, single-layer gratings suggest compact filter performances, although possible use of metasurfaces might improve them, e.g., by allowing the use of narrower incident beams.

References

1. L. Dettwiller, P. Chavel, Optical spatial frequency filtering using interferences. J. Opt. Soc. Am. A **1**, 18–27 (1984)
2. D. Schurig, D.R. Smith, Spatial filtering using media with indefinite permittivity and permeability tensors. Appl. Phys. Lett. **82**, 2215–2217 (2003)
3. A. Sentenac, A.-L. Fehrembach, Angular tolerant resonant grating filters under oblique incidence. J. Opt. Soc. Am. A **22**, 475–480 (2005)
4. R. Rabady, I. Avrutsky, Experimental characterization of simultaneous spatial and spectral filtering by an optical resonant filter. Opt. Lett. **29**, 605–607 (2004)
5. I. Moreno, J.J. Araiza, M. Avedano-Alejo, Thin film spatial filters. Opt. Lett. **30**, 914–916 (2005)
6. O.F. Siddiqui, G. Eleftheriades, Resonant modes in continuous metallic grids over ground and related spatial-filtering applications. J. Appl. Phys. **99**, 083102 (2006)
7. V. Purlys, L. Maigyte, D. Gailevicius, M. Peckus, M. Malinauskas, R. Gadonas, K. Staliunas, Spatial filtering by axisymmetric photonic microstructures. Opt. Lett. **39**, 929–932 (2014)
8. A.E. Serebryannikov, A.Y. Petrov, E. Ozbay, Toward photonic-crystal based spatial filters with wide-angle ranges of total transmission. Appl. Phys. Lett. **94**, 181101 (2009)
9. L. Maigyte, K. Staliunas, Spatial filtering with photonic crystals. Appl. Phys. Rev. **2**, 011102 (2015)
10. V. Purlys, L. Maigyte, D. Gailevicius, M. Peckus, M. Malinauskas, K. Staliunas, Spatial filtering by chirped photonic crystals. Phys. Rev. A **87**, 033805 (2013)
11. A.E. Serebryannikov, E. Colak, A. Petrov, P.V. Usik, E. Ozbay, Multifrequency spatial filtering: a general property of two-dimensional photonic crystals. Photon. Nanostruct. Fundam. Appl. **18**, 1–9 (2016)
12. J.H. Wu, L.K. Ang, A.Q. Liu, H.G. Teo, C. Lu, Tunable high-Q photonic-bandgap Fabry–Perot resonator. J. Opt. Soc. Am. B **22**, 1770–1777 (2005)
13. Y.J. Lee, J. Yeo, R. Mittra, W.S. Park, Application of electromagnetic bandgap (EBG) superstrates with controllable defects for a class of patch antennas as spatial angular filters. IEEE Trans. Antennas Propag. **53**, 224–235 (2005)
14. R. Pico, I. Perez-Arjona, V.J. Sanchez-Morcillo, K. Staliunas, Evidences of spatial (angular) filtering of sound beams by sonic crystals. Appl. Acoust. **74**, 945–948 (2013)
15. E.H. Cho, H.-S. Kim, B.-H. Cheong, O. Prudnikov, W. Xianyua, J.-S. Sohn, D.-J. Ma, H.-J. Choi, N.-C. Park, Y.-P. Park, Two-dimensional photonic crystal color filter development. Opt. Express **17**, 8621–8629 (2009)
16. B.-H. Cheong, O.N. Prudnikov, E. Cho, H.-S. Kim, J. Yu, J.-S. Cho, H.-J. Choi, S.T. Shin, High angular tolerant color filter using subwavelength grating. Appl. Phys. Lett. **94**, 213104 (2009)
17. E. Colak, A.O. Cakmak, A.E. Serebryannikov, E. Ozbay, Spatial filtering using dielectric photonic crystals at beam-type illumination. J. Appl. Phys. **108**, 113106 (2010)
18. M. Born, E. Wolf, *Principles of Optics*, 4th edn. (Pergamon Press, Oxford, 1970)
19. A.E. Serebryannikov, E. Ozbay, P.V. Usik, Defect-mode-like transmission and localization of light in photonic crystals without defects. Phys. Rev. B **82**, 165131 (2010)
20. K. Sakoda, *Optical Properties of Photonic Crystals* (Springer, Berlin, 2001)

21. J. Li, T.P. White, L. O'Faolain, A. Gomez-Iglesias, T.F. Krauss, Systematic design of flat band slow light in photonic crystal waveguides. Opt. Express **16**, 6227–6232 (2008)
22. A.E. Serebryannikov, A.O. Cakmak, E. Colak, H. Caglayan, H. Kurt, E. Ozbay, Multiple slow waves and relevant transverse transmission and confinement in chirped photonic crystals. Opt. Express **22**, 21806–21819 (2014)
23. S. Foteinopoulou, C.M. Soukoulis, Electromagnetic wave propagation in two-dimensional photonic crystals: a study of anomalous refractive effects. Phys. Rev. B **72**, 165112 (2005)
24. K. Wiesemann, A short introduction to plasma physics. CERN Yellow Report CERN-2013-007, pp. 85–122 (2013). doi:10.5170/CERN-2013-007.85
25. L.V. Alekseyev, E.E. Narimanov, T. Tumkur, H. Li, Yu.A. Barnakov, M.A. Noginov, Uniaxial epsilon-near-zero metamaterial for angular filtering and polarization control. Appl. Phys. Lett. **97**, 131107 (2010)
26. A. Alu, M.G. Silveirinha, A. Salandrino, N. Engheta, Epsilon-near-zero metamaterials and electromagnetic sources: tailoring the radiation phase pattern. Phys. Rev. B **75**, 155410 (2007)
27. B.T. Schwartz, R. Piestun, Total external reflection from metamaterials with ultralow refractive index. J. Opt. Soc. Am. B **20**, 2448–2453 (2003)
28. N. Kinsley, C. DeVault, J. Kim, M. Ferrera, V.M. Shalaev, A. Boltasseva, Epsilon-near-zero Al-doped ZnO for ultrafast switching at telecom wavelengths. Optica **2**, 616–622 (2015)
29. D.A. Woods, C.D. Bain, Total internal reflection spectroscopy for studying soft matter. Soft Matter **10**, 1071–1096 (2014)
30. C. Rizza, A. Ciattoni, E. Spinozzi, L. Colombo, Terahertz active spatial filtering through optically tunable hyperbolic metamaterials. Opt. Lett. **37**, 3345–3347 (2012)
31. A.E. Serebryannikov, One-way diffraction effects in photonic crystal gratings made of isotropic materials. Phys. Rev. B **80**, 155117 (2009)
32. C. Luo, S.G. Johnson, J.D. Joannopoulos, J.B. Pendry, All-angle negative refraction without negative effective index. Phys. Rev. B **65**, 201104(R) (2002)
33. R. Petit (Ed.), *Electromagnetic Theory of Gratings* (Springer, Berlin, 1980)
34. A.E. Serebryannikov, P. Lalanne, A.Yu. Petrov, E. Ozbay, Wide-angle reflection-mode spatial filtering and splitting with photonic crystal gratings and single-layer rod gratings. Opt. Lett. **39**, 6193–6196 (2014)
35. D.R. Smith, N. Kroll, Negative refractive index in left-handed materials. Phys. Rev. Lett. **85**, 2933–2936 (2000)
36. H. Kosaka, T. Kawashima, A. Tomita, M. Notomi, T. Tamamura, T. Sato, S. Kawakami, Self-collimating phenomena in photonic crystals. Appl. Phys. Lett. **74**, 1212–1214 (1999)
37. M.C. Hutley, *Diffraction Gratings* (Academic Press, London, 1982)
38. Ph. Lalanne, S. Astilean, P. Chavel, E. Cambril, H. Launois, Design and fabrication of blazed binary diffractive elements with sampling periods smaller than the structural cutoff. J. Opt. Soc. Am. A **16**, 1143–1156 (1999)
39. C. Sauvan, Ph. Lalanne, L.M.-S. Lee, Broadband blazing with artificial dielectrics. Opt. Lett. **29**, 1593–1595 (2004)
40. E. Colak, A.E. Serebryannikov, P.V. Usik, E. Ozbay, Diffraction inspired unidirectional and bidirectional beam splitting in defect-containing photonic structures without interface corrugations. J. Appl. Phys. **119**, 193108 (2016)
41. A.E. Serebryannikov, A. Lakhtakia, E. Ozbay, Single and cascaded, magnetically controllable metasurfaces as terahertz filters. J. Opt. Soc. Am. B **33**, 834–841 (2016)

Andriy E. Serebryannikov received Diploma in Physics and Technology (1990) and Ph.D. degree in Radio Physics (1996) from Kharkiv Polytechnic University and Kharkiv National University (both Kharkiv, Ukraine), respectively. In 2014, he joined Adam Mickiewicz University in Poznan, Poland. He has published 90 journal articles and more than 50 conference papers.

His current research interests include theory and applications of metasurfaces, metamaterials, photonic crystals, surface plasmons, polarization manipulation, and magnonics.

Ekmel Ozbay received M.S. and Ph. D. degrees from Stanford University in electrical engineering, in 1989 and 1992. He worked as a postdoctoral research associate in Stanford University and as a scientist in Iowa State University. He joined Bilkent University (Ankara, Turkey) in 1995, where he is currently a full professor in the Department of Electrical and Electronics Engineering.

His research in Bilkent involves nanophotonics, nanometamaterials, nanoelectronics, nanoplasmonics, nanodevices, photonic crystals, GaN/AlGaN MOCVD growth, fabrication and characterization of GaN-based devices, and high-speed optoelectronics. He is the 1997 recipient of the Adolph Lomb Medal of Optical Society of America and 2005 European Union Descartes Science award. He worked as an editor for Scientific Reports, Optics Letters, Photonics and Nanostructures Fundamental Applications, and IEEE Journal of Quantum Electronics. He has published 390+ articles in SCI journals. His papers have received 11000+ SCI citations with an SCI h-index of 51. He has given 135+ invited talks in international conferences.